Layered localization in a chaotic optical cavity

Yu-Zhong Gu,[1] Li-Kun Chen,[1] Yan-Jun Qian,[1] Qihuang Gong,[1,2,3] Qi-Tao Cao,[1,*] and Yun-Feng Xiao[1,2,3]

[1]*State Key Laboratory for Mesoscopic Physics and Frontiers Science Center for Nano-Optoelectronics, School of Physics, Peking University, 100871 Beijing, China*

[2]*Collaborative Innovation Center of Extreme Optics, Shanxi University, Taiyuan 030006, China*

[3]*Peking University Yangtze Delta Institute of Optoelectronics, Nantong, Jiangsu 226010, China*

(Received 31 July 2020; revised 28 October 2020; accepted 19 November 2020; published 14 December 2020)

We propose and demonstrate the localization of resonant modes in a Limaçon optical microcavity with layered phase space involving both major and minor partial barriers. By regulating the openness of the cavity through the refractive index control, the minor partial barriers, which do not directly confine the long-lived resonant modes, are submerged successively into the leaky region. During the invalidation process of the minor partial barriers, it is found that the quality factor and the conjugate momentum of the resonant modes exhibit changes with the emergence of turning points. Such phenomena are attributed to the joint confinement effect by the minor partial barriers together with the major one in the layered phase space. This paper helps to improve the understanding of complex dynamics, and sheds light on the fine design of photonic devices with high performance.

DOI: 10.1103/PhysRevE.102.062208

I. INTRODUCTION

Localization of resonant states is crucial in the study of dynamical systems for revealing the quantum feature of stochastic motions [1–6]. Within a fully chaotic region, a ubiquitous localization mechanism is provided by partial barriers in the phase space [7–10], which has been investigated in various systems such as nonlinear oscillators [6], chaotic billiards [10–12], and ionizations [13–15]. The partial barrier is a ubiquitous structure in chaotic phase space, formed by homoclinic orbits, cantori, or periodic orbits [7,8]. For classical dynamics, a partial barrier imperfectly divides the chaotic region into two nearly isolated subregions. All motions crossing the partial barrier must pass through a specific area named as flux determined by the partial barrier. In the quantum regime, a wave packet with an extended size hardly resolves the flux due to wave effects, which suppresses the classical transition across the partial barrier [10,16]. Therefore, the nearly invariant subregions divided by the partial barrier provide resonance zones for wave localizations [8,10], even though the holistic classical dynamics does not support any regular orbits with strong coherence. In this view, long-lived resonant states can also exist in the chaotic phase space with the assistance of partial barriers.

In previous works, this localization mechanism is only considered with the existence of a single partial barrier [9,12,16], by which a resonant mode is directly confined in the quantum regime [10]. However, for a real chaotic system, there generally exist multiple partial barriers forming a layered structure in the phase space. The impact on the localization of resonant modes by multiple partial barriers has been still elusive so far. In this paper, we propose and demonstrate the layered localization of an open system in a Limaçon optical cavity in the quantum regime. Here the phase space is divided by several homoclinic partial barriers. The long-lived resonant modes are mainly governed by one major partial barrier, which bounds most of the mode projection in the phase space [10]. Other partial barriers, named as minor partial barriers, locate between the major one and the leaky region (Fig. 1). By adjusting the cavity refractive index to control the openness of the system, we investigate the localization of whispering gallery modes (WGMs) [17] through tracing their quality factors (Q) and the averaged conjugate momentum. During the submersion process of the minor partial barriers into the leaky region, explicit turning points of the Q factor and conjugate momentum are observed, revealing the additional localization effect brought by the minor partial barriers. Moreover, through varying the mode number and the deformation of the cavity, it is found that this turning point is influenced by both the flux of the partial barrier and the size of the Planck cell.

II. CHAOTIC OPTICAL CAVITY SYSTEM

The chaotic system used here is an asymmetric optical microcavity which provides a significant platform for the study of both classical and wave chaos [17–21], benefiting from its phase space with multitudinous structures and the easy control of openness. In the past decades, numerous advanced developments have been witnessed in asymmetric microcavities, such as dynamical tunneling [22–24], non-Hermitian physics [25,26], low-coherence lasers [27–29], and nonlinear optics [30,31]. The classical dynamics of the light inside a chaotic asymmetric optical cavity is described by the billiard model, which records the reflection position s and the incident angle χ for each reflection of the propagating light [Fig. 1(a)]. The real-space trajectory of the light in the cavity can be mapped into the phase space (Poincaré surface of the section) with the

*caoqt@pku.edu.cn

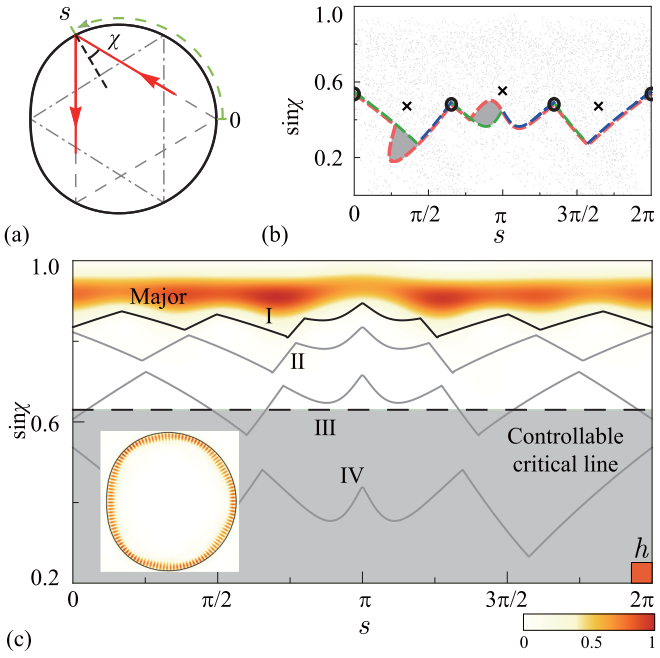

FIG. 1. (a) Schematic diagram of the billiard model for a Limaçon cavity. As an example, hyperbolic (dashed line) and elliptic (dot-dashed line) three-period orbits in real space are given. (b) Poincaré surface of section with chaotic dynamics. The corresponding three-period orbits are also given in the phase space, marked with circles (hyperbolic) and crosses (elliptic). (c) The Husimi projection (heat map) of a WGM is confined by the major partial barrier (black curve). Partial barriers of six-, five-, four-, and three-period orbits are marked with I, II, III, and IV, respectively. The dashed line denotes the critical line of total internal reflection, which defines the leaky region (gray region). The size of Planck cell h is given in the lower-right corner for reference, which represents the relative size of the wave packet. Inset: Field distribution of a typical fundamental WGM in real space.

arc length s normalized to 2π and the corresponding conjugate momentum $\sin\chi$ [32], as shown in Fig. 1(b).

Here we choose a Limaçon shaped cavity with an easily modulated phase space, which has been extensively researched in various fields [33–37]. The cavity boundary shape is described by the function in polar coordinates (r, ϕ) : $r(\phi) = 1 + \varepsilon\cos\phi$, where ε is the deformation parameter. The deformation parameter ε is large enough ($\varepsilon = 0.43$ if not indicated otherwise) to ensure that the phase space is highly chaotic. In this case, the impact of remaining island structures under the wave effect can be ignored [33], so that the stickiness originated from the island structure [38] can be avoided. The phase space is divided by the homoclinic partial barriers which are formed by the stable and unstable manifolds of the hyperbolic periodic orbits [7]. The stable (unstable) manifold is the set of points converging to the periodic orbits in forward (backward) evolution [32,39], marked by the blue (green) dashed curves in Fig. 1(b). The corresponding flux A [shaded area in Fig. 1(b)], characterizing the transition property of the partial barrier, is derived from the area enclosed by the partial barrier and its one-time backward mapping [red curves in Fig. 1(b)] [8]. In addition, the optical cavity is a partially open system, the leakage of which is determined by the refractive loss. As shown in Fig. 1(c), the leaky region in the phase space is defined by the critical line corresponding to the critical total internal reflection $\sin\chi_c = 1/n$, where n is the relative refractive index between the cavity and the external medium.

Generally, the Husimi projection is employed to characterize a resonant mode in the phase space [40], as shown in Fig. 1(c). It is found that the major partial barrier I efficiently confines the fundamental WGM, while the existing minor partial barriers, i.e., II, III, and IV, are away from the resonant mode in the phase space. Despite the tiny overlap with the mode distribution, the minor partial barriers also bring an additional localization effect.

III. LAYERED LOCALIZATION MANIFESTED BY GLOBAL PROPERTIES

In order to investigate the localization from the minor partial barriers, we regulate the openness of the asymmetric cavity and monitor the global properties of the resonant modes. This is because the openness of the system connects the transient and the persistent dynamics [41], and the localization representing asymptotic behaviors is severely modulated by the short-time dynamics close to the leaky region. As a technical method, the openness of the system is manipulated by changing the refractive index n to control the critical line, and the corresponding influence on the localization can be explicitly reflected in the form of quality factors and conjugate momentum of the resonant modes.

A. Quality factor

First, we investigate the Q factor of fundamental WGMs, which instructively manifests the decay rate and the localization of the mode. By employing the boundary element method [42], the field distributions and Q factors of the long-lived resonant modes are obtained [43]. Then we trace the WGMs with the same angular mode number m during the variation of the critical line, which is mostly confined by the partial barrier I marked as the black curve in Fig. 2(b). The mode number m for fundamental WGMs in an asymmetric cavity is defined with the number of maxima along the azimuthal direction divided by 2. Note the field distribution of WGMs in the real space [inset of Fig. 1(c)] is characteristic to ensure that the same mode is traced while varying the openness. Figure 2(a) shows the dependence of the Q factors on the critical line with different mode numbers m. It is found that for a fixed mode number, the Q factors tend to descend with the lift of the critical line due to the increment of system openness, and commonly exhibit an explicit turning point in the blue region. As an example, the turning points of the Q factors with the mode number $m = 65$ is plotted in the inset of Fig. 2(a). Bounds of the blue region are defined by the turning points for $m = 60$ and 69 curves, in which resonant modes take additional leakage along with the rising critical line. For a more intuitive aspect, the blue region containing the turning points is found coincident with partial barriers II, as shown by the blue curve in Fig. 2(b). Owing to the little change in radiation loss induced by material refractive index, the emergence of the turning points implies that the

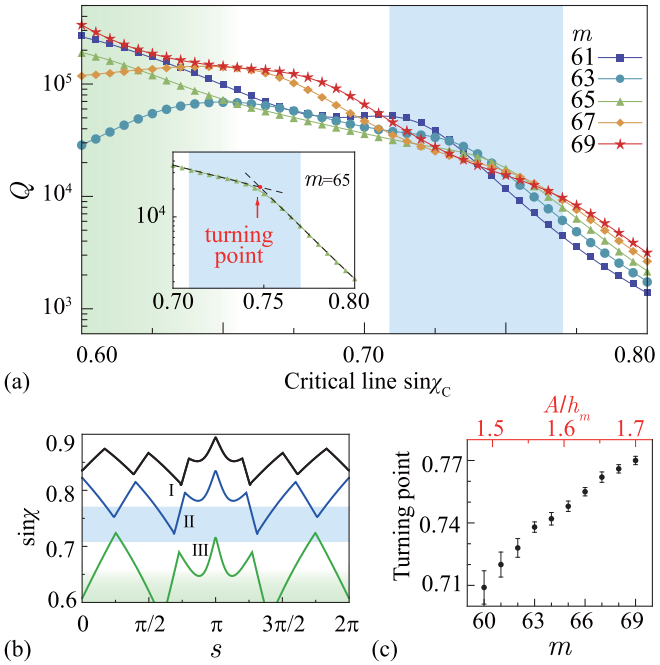

FIG. 2. (a) Q factors of WGMs depending on the critical line $\sin\chi_C$. The WGMs with different mode numbers m are mostly confined by the major partial barrier I. Inset: A specific illustration of the turning point in the blue region. The turning point is defined as the intersection of fitting slopes. (b) The phase space marked with the blue and gradient green shadows, which correspond to the regions with same color in (a). (c) Turning points of Q and fitting errors in the blue region (partial barrier II) vs the mode number m and the ratio between flux A and Planck cell h_m.

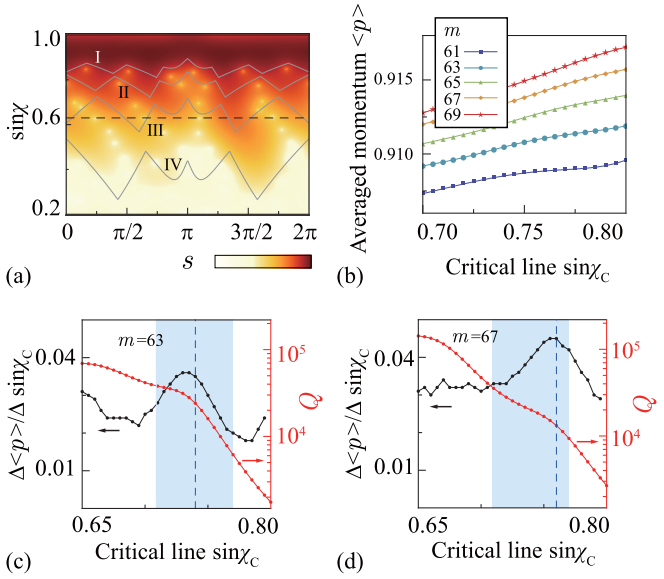

FIG. 3. (a) Husimi projection of a typical WGM confined by partial barrier I in logarithmic scale. (b) Averaged momentum $\langle p\rangle$ of the Husimi distribution depending on the critical line $\sin\chi_C$ with different mode numbers. (c, d) Comparison between the Q factors (red curve) and the symmetric derivative of the averaged momentum $\Delta\langle p\rangle/\Delta\sin\chi_C$ (black curve) for mode number (c) $m = 63$ and (d) $m = 67$. The blue dashed line marks the position of the turning point.

additional localization brought by the minor partial barrier takes responsibility for the emergence of turning points. When the critical line lifts high enough to cover a partial barrier, the additional localization of this partial barrier becomes void. Then the leakage process of the WGMs encounters a transition and turns out to be the turning points in the slopes of Q factors. Additionally, it is also found that the slopes at the green region show weak correlations, where a turning point ought to emerge due to the localization effect of partial barrier III. However, other low Q modes with higher radial number living in the resonance zone between partial barriers II and III induce modal coupling effect to fundamental WGMs. The modal coupling takes undesired interference to the leakage process [44–46], which surpasses the localization effect brought by the partial barrier III and results in the weak correlation in the slopes. In contrast, the modes localized between partial barriers I and II are far detuned from the fundamental WGMs. Therefore, there is no modal coupling for the blue region case, for which we will focus on this region in the rest of this paper.

Furthermore, we note that the position of turning points in the blue region exhibits a strong dependence on the mode number m shown in Fig. 2(c). This localization is tightly related to the transition property of partial barriers, which is governed by the ratio between the flux of the partial barrier A and the size of Planck cell h_m [16]. In our case, A is the flux of the partial barriers II, which is constant for the specified boundary condition. The size of Planck cell $h_m = 1/nkR$ is varied with different mode numbers m, where k denotes the wave vector in vacuum and R denotes averaged radius of cavity in the polar coordinate. Especially, the product nkR keeps nearly invariant for a fixed mode number m, so that the size of Planck cell h_m is uniformed with the refractive index n but dependent with the mode number m. For our system, the ratio A/h_m is comparable with 1 representing a proper wave effect, in which the transition rates through the partial barriers are explicitly modulated by the ratio A/h_m [10,16]. Here the dependence of the turning point on the ratio A/h_m is plotted in Fig. 2(c), exhibiting a positive correlation. This phenomenon can be understood as that the transition rates rise with a smaller Planck cell h_m for the shrinkage of wave effect, resulting in the weak localization. As a result, the global properties of the system with smaller h_m are less affected by the additional localization effect of the partial barrier, and need larger openness to manifest the dramatic change in Q factors.

B. Conjugate momentum

Besides the investigation of the Q factors, the conjugate momentum of the resonant modes is also explored in the phase space. As shown in Fig. 3(a), the Husimi projection of a typical WGM shows a layered distribution in the logarithmic scale, the contours of which are coincident with partial barriers. Quantitatively, we calculate the averaged momentum $\langle p\rangle = \iint pH(s,p)dsdp$ with the conjugate momentum $p = \sin\chi$ and Husimi projection $H(s,p)$. Following the same instructions as tracing the Q factor of the WGMs, we obtain the trend of the averaged momentum with the changing of the critical line shown in Fig. 3(b). With the lift of the critical

line, the remanent tail of the projection close to the leaky region vanishes gradually, which naturally results in the rising trend of the averaged momentum. To reveal the variation in the momentum of the resonant mode, the symmetric derivative of the averaged momentum is investigated and compared with Q factors as shown in Figs. 3(c) and 3(d). As for the WGMs with different mode numbers m, both of the symmetric derivative curves exhibit single major peaks in the blue region, which are exactly coincident with the turning point of Q factors with respect to partial barrier II. This result implies that the minor partial barriers have impacts on the holistic dynamics literally.

The features of momentum curves can be well explained by the layered structure with partial barriers. In our system, the leakage of modes is characterized by the lowest partial barrier beyond the critical line. For example, in Fig. 3, the critical line changes from the level below the partial barrier II to approach the partial barrier I. In this process, the leakage is initially governed by the partial barrier II. The averaged momentum grows evenly due to the enlargement of the leaky region until the critical line touches the partial barrier II. When the critical line reaches the partial barrier II, its additional localization is destroyed and the leakage experiences a dramatic change, resulting in a sudden rise in the averaged momentum. After this, the leakage will be governed by the partial barrier I and the growth of averaged momentum tends to be even. As a result, the symmetric derivative curves of averaged momentum commonly show peaks corresponding to the turning point of Q factors, which represents the invalidation of a minor partial barrier.

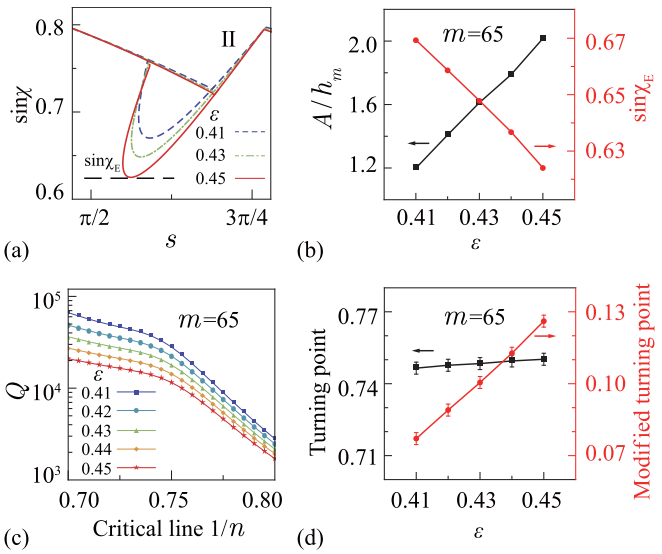

FIG. 4. (a) The incoming fluxes of partial barriers II in the phase space with different deformation parameters ε. (b) The ratio A/h_m vs the deformation parameter ε. The corresponding lower edge of the incoming flux $\sin\chi_E$ is also marked with the red curve. The mode number is fixed as $m = 65$. (c) Quality factors of WGMs depending on the critical line $\sin\chi_C$ with fixed mode number m and different deformation parameters ε. (d) The Q turning point and fitting error in the partial barrier II region vs the deformation parameter ε. A modified result with the red curve is obtained by considering the relative position with the edge $\sin\chi_E$.

IV. VARIANCE OF THE TURNING POINT

At last, we present the determinant of the localization effect of a single partial barrier. As mentioned in Fig. 2(c), the drift of turning points is supposed to be caused by the changing ratio of flux to Planck cell A/h_m. Different from variation in the Planck cell shown in Fig. 2, now we control the flux A by choosing different deformation parameter ε. Figure 4(a) illustrates the incoming fluxes of the five-period partial barriers (II) with different deformation parameters ε in the phase space. The profiles of partial barriers are roughly the same but the incoming fluxes are quite different, and the corresponding ratio A/h_m is given in Fig. 4(b). For cavities with larger deformation parameters, the dynamics is more disordered, so that the corresponding fluxes are larger than those with smaller deformation. Then we focus on a single WGM (m=65) to investigate the change of turning points with different deformation parameters following the same instructions in Fig. 2. The variation of Q factors with the changing critical line is illustrated in Fig. 4(c), and the corresponding turning points of these curves are given in Fig. 4(d).

However, unlike the results in Fig. 2(c), the turning points keep almost invariant with the change of ratio A/h_m. This phenomenon is mainly attributed to two destructive effects caused by the enlarged flux and the lowered offset. As for the latter, specifically, the flux in the case of a cavity with a larger deformation parameter has a lower edge $\sin\chi_E$ marked in Fig. 4(a), which is supposed to touch the critical line earlier at a lower position of $\sin\chi$. Therefore, the turning points turn out to be at a lower position of $\sin\chi$, which counteracts the effect by the increased ratio A/h_m shown in Fig. 2(c). By recording the relative distance from the edge $\sin\chi_E$ to the turning point, a modified turning point is estimated in Fig. 4(d) simultaneously. The modified result shows a same correlation with Fig. 2(c), implying that the ratio A/h_m indeed takes responsibility to the turning point in this process.

V. DISCUSSION AND CONCLUSION

The method to investigate the layered localization by partial barriers is also realizable in real experiments. It is realistic to reach a wide range of critical line tuning by employing a jet asymmetric microcavity or putting the asymmetric microcavity in a liquid environment, where the relative refractive index can be easily controlled. Similar setups such as liquid jets [24,47] have been realized to investigate the unidirectional emission and dynamical tunneling in asymmetric microcavities. It is achievable to analyze the localization of resonant modes through monitoring mode Q factors from the transmission spectra of a passive optical cavity or measuring the lasing threshold of an active cavity.

In summary, we propose and demonstrate the localization within a layered phase space in the quantum regime by utilizing a chaotic optical cavity. Besides the major partial barrier directly confining the resonant modes, the minor partial barriers also take joint confinement effect for localization of resonant modes. The localizing capacity of the minor partial barrier is demonstrated and studied by controlling the openness of the system and observing the global performance of resonant modes, i.e., Q factor and averaged conjugate momen-

tum. Consequently, these global properties present turning points as the minor partial barrier gradually submerges into the leaky region. In addition, the turning point shows a dependence on the flux A and the size of Planck cell h_m. Noted that although this paper mainly focuses on the three-layer structure divided by one major and one minor partial barrier, this result is the simplest model for the effects of layered partial barriers and can be readily extended to the structure with more minor partial barriers. This demonstrated layered localization by multiple partial barriers is of great importance for understanding the complex dynamics in fundamental researches and can be utilized in the design of functional cavities with flexible emission features and exceptional modes.

For future researches, there exist the following unsolved problems and challenges.

(1) The dependence of the turning point and the ratio A/h_m is phenomenologically explained in this paper, while a quantitative prediction is required for this dependence in physics.

(2) The optical cavity in this paper is a partially open system governed by Fresnel's law, while a chaotic system with an absolutely absorbed leakage can also be investigated for the layered localization [9,41,48,49].

(3) The dynamical tunneling [22,50] is ignored in this paper but makes a difference in the localization of resonant modes, which can be impacted by the changing Planck cell.

(4) There is a small rising tendency for Q curves before the turning point we defined in Fig. 2, which cannot be explained by our model. Some other mechanisms, e.g., external coupling [51], are required to be considered in future works.

ACKNOWLEDGMENT

The authors thank Y.-Q. Nie, D. Xu, X.-C. Yu, H.-J. Chen, and P.-J. Zhang for helpful discussions. This project is supported by the National Key Research and Development Program of China (Grants No. 2016YFA0301302 and No. 2018YFB2200401), the National Natural Science Foundation of China (Grants No. 11825402, No. 11654003, No. 61435001, and No. 12041602), Beijing Academy of Quantum Information Sciences (Grant No. Y18G20), Key Research and Development Program of Guangdong Province (Grant No. 2018B030329001), and the High-Performance Computing Platform of Peking University.

[1] S. Fishman, D. R. Grempel, and R. E. Prange, Phys. Rev. Lett. **49**, 509 (1982).
[2] E. J. Heller, Phys. Rev. Lett. **53**, 1515 (1984).
[3] F. Borgonovi, G. Casati, and B. Li, Phys. Rev. Lett. **77**, 4744 (1996).
[4] H. Schomerus and J. Tworzydlo, Phys. Rev. Lett. **93**, 154102 (2004).
[5] J. P. Keating, M. Novaes, S. D. Prado, and M. Sieber, Phys. Rev. Lett. **97**, 150406 (2006).
[6] R. C. Brown and R. E. Wyatt, Phys. Rev. Lett. **57**, 1 (1986).
[7] J. D. Meiss, Rev. Mod. Phys. **64**, 795 (1992).
[8] J. D. Meiss, Chaos **25**, 097602 (2015).
[9] M. J. Körber, A. Bäcker, and R. Ketzmerick, Phys. Rev. Lett. **115**, 254101 (2015).
[10] J.-B. Shim, J. Wiersig, and H. Cao, Phys. Rev. E **84**, 035202(R) (2011).
[11] J. B. Shim, S.-B. Lee, S.-W. Kim, S.-Y. Lee, J. Yang, S. Moon, J.-H. Lee, and K. An, Phys. Rev. Lett. **100**, 174102 (2008).
[12] K. Burke and J. U. Nöckel, Phys. Rev. A **100**, 063829 (2019).
[13] K. Burke, K. A. Mitchell, B. Wyker, S. Ye, and F. B. Dunning, Phys. Rev. Lett. **107**, 113002 (2011).
[14] N. Mertig and A. Shudo, Phys. Rev. E **97**, 042216 (2018).
[15] S. W. Kim and H.-W. Lee, Phys. Rev. E **61**, 5124 (2000).
[16] M. Michler, A. Bäcker, R. Ketzmerick, H.-J. Stöckmann, and S. Tomsovic, Phys. Rev. Lett. **109**, 234101 (2012).
[17] H. Cao and J. Wiersig, Rev. Mod. Phys. **87**, 61 (2015).
[18] J. U. Nöckel and A. D. Stone, Nature (London) **385**, 45 (1997).
[19] C. F. Gmachl, F. Capasso, E. E. Narimanov, J. U. Nöckel, A. D. Stone, J. Faist, D. L. Sivco, and A. Y. Cho, Science **280**, 1556 (1998).
[20] T. Harayama and S. Shinohara, Laser Photonics Rev. **5**, 247 (2011).
[21] Q. Song, Sci. China: Phys., Mech. Astron. **62**, 074231 (2019).
[22] A. Bäcker, R. Ketzmerick, S. Löck, J. Wiersig, and M. Hentschel, Phys. Rev. A **79**, 063804 (2009).
[23] S. Shinohara, T. Harayama, T. Fukushima, M. Hentschel, T. Sasaki, and E. E. Narimanov, Phys. Rev. Lett. **104**, 163902 (2010).
[24] J. Yang, S.-B. Lee, S. Moon, S.-Y. Lee, S. W. Kim, T. Thi Anh Dao, J.-H. Lee, and K. An, Phys. Rev. Lett. **104**, 243601 (2010).
[25] S.-B. Lee, J. Yang, S. Moon, S.-Y. Lee, J.-B. Shim, S. W. Kim, J.-H. Lee, and K. An, Phys. Rev. Lett. **103**, 134101 (2009).
[26] C.-H. Yi, J. Kullig, and J. Wiersig, Phys. Rev. Lett. **120**, 093902 (2018).
[27] B. Redding, A. Cerjan, X. Huang, M. L. Lee, A. D. Stone, M. A. Choma, and H. Cao, Proc. Natl. Acad. Sci. USA **112**, 1304 (2015).
[28] S. Sunada, S. Shinohara, T. Fukushima, and T. Harayama, Phys. Rev. Lett. **116**, 203903 (2016).
[29] S. Bittner, S. Guazzotti, Y. Zeng, X. Hu, H. Yilmaz, K. Kim, S. S. Oh, Q. J. Wang, O. Hess, and H. Cao, Science **361**, 1225 (2018).
[30] X. Jiang, L. Shao, S. Zhang, X. Yi, J. Wiersig, L. Wang, Q. Gong, M. Lončar, L. Yang, and Y. Xiao, Science **358**, 344 (2017).
[31] H.-J. Chen, Q.-X. Ji, H. Wang, Q.-F. Yang, Q.-T. Cao, Q. G. Gong, X. Yi, and Y.-F. Xiao, Nat. Commun. **11**, 2336 (2020).
[32] A. J. Lichtenberg and M. A. Lieberman, *Regular and Chaotic Dynamics* (Springer-Verlag, Berlin, 1992).
[33] H. R. Dullin, and A. Bäcker, Nonlinearity **14**, 1673 (2001).
[34] J. Wiersig and M. Hentschel, Phys. Rev. Lett. **100**, 033901 (2008).

[35] Q. Song, W. Fang, B. Liu, S.-T. Ho, G. S. Solomon, and H. Cao, Phys. Rev. A **80**, 041807(R) (2009).
[36] C. Yan, Q. J. Wang, L. Diehl, M. Hentschel, J. Wiersig, N. Yu, C. Pflügl, F. Capasso, M. A. Belkin, T. Edamura, M. Yamanishi, and H. Kan, Appl. Phys. Lett. **94**, 251101 (2009).
[37] B. Redding, L. Ge, Q. Song, J. Wiersig, G. S. Solomon, and H. Cao, Phys. Rev. Lett. **108**, 253902 (2012).
[38] E. G. Altmann, Phys. Rev. A **79**, 013830 (2009).
[39] H. G. L. Schwefel, N. B. Rex, H. E. Tureci, R. K. Chang, A. D. Stone, T. Ben-Messaoud, and J. Zyss, J. Opt. Soc. Am. B **21**, 923 (2004).
[40] M. Hentschel, H. Schomerus, and R. Schubert, Europhys. Lett. **62**, 636 (2003).
[41] E. G. Altmann, J. S. E. Portela, and T. Tél, Rev. Mod. Phys. **85**, 869 (2013).
[42] J. Wiersig, J. Opt. **5**, 53 (2003).
[43] The precision of the numerical result is determined by the number of boundary elements, which is set as 1200 in our simulation. The quality factor $Q = kW/P$ is obtained by dividing the outgoing energy flux P into the integral of inner energy W with k the wave vector in vacuum.
[44] Q. Song, L. Ge, A. D. Stone, H. Cao, J. Wiersig, J.-B. Shim, J. Unterhinninghofen, W. Fang, and G. S. Solomon, Phys. Rev. Lett. **105**, 103902 (2010).
[45] Q. Song, C. Zeng, and S. Xiao, Phys. Rev. A **87**, 013831 (2013).
[46] Y.-D. Yang, S.-J. Wang, and Y.-Z. Huang, Opt. Express **17**, 23010 (2009).
[47] S.-Y. Lee and K. An, Phys. Rev. A **83**, 023827 (2011).
[48] L. Wang, D. Lippolis, Z.-Y. Li, X.-F. Jiang, Q. Gong, and Y.-F. Xiao, Phys. Rev. E **93**, 040201(R) (2016).
[49] D. Lippolis, L. Wang, and Y. F. Xiao, Phys. Rev. E **96**, 012217 (2017).
[50] A. Bäcker, R. Ketzmerick, S. Löck, and L. Schilling, Phys. Rev. Lett. **100**, 104101 (2008).
[51] J. Wiersig, Phys. Rev. Lett. **97**, 253901 (2006).